Investigation of Wet-Spun Acrylic Fiber Morphology by Membrane Technology Techniques

S. J. LAW and S. K. MUKHOPADHYAY*

Department of Textile Industries, University of Leeds, Leeds LS2 9JT, United Kingdom

SYNOPSIS

The as-formed structure of wet-spun acrylic fiber from the sodium thiocyanate system has been probed, exploiting a number of techniques developed in the membrane industry. The use of flat membrane geometry in the study of wet-spun fibers has been proven to be valid. The calculation of average pore dimensions in the surface of acrylic membranes by a hydraulic permeability method has agreed well with microscopic examination. The skin layer present on both fibers and membranes has been shown to be structurally isotropic for the extruded fiber by a novel polarized infrared microspectroscopy technique. The consequences of this in downstream processing are discussed. © 1996 John Wiley & Sons, Inc.

INTRODUCTION

Acrylic fibers have been commercially produced now for nearly 50 years. In recent times, a decline in acrylic consumption has been experienced but it still remains a significant commodity, despite the withdrawal recently of major players, notably DuPont.

From a technical point of view, no other man-made fiber can have such a diversity of commercial production routes, from dry, through dry-wet, to wet spinning, utilizing solvents from dimethylformamide through zinc chloride to nitric acid.

The structure of acrylic fibers can be considered on two levels. First, there is the molecular organization which gives rise to features generally but not exclusively observed by diffraction techniques, typically wide-angle X-ray diffraction (WAXRD). Second, the gross morphology arising initially from the way the polymer is regenerated from solution, and later affected by downstream processing, can be studied microscopically.

A wealth of data concerning the molecular structure of acrylic fibers has been generated over the years, covering both intrachain and interchain organizations.[1-6] The consensus appears to be that polyacrylonitrile (PAN), and its copolymer relatives adopt an irregular helical configuration with the C≡N dipoles arranged so as to minimize repulsion between near neighbors. Chains in an oriented fiber pack roughly parallel, again so as to minimize dipole–dipole repulsion. Orthorhombic or hexagonal unit cells have been suggested, and there exists only lateral order, with no axial chain periodicity. Such a structure has been termed "paracrystalline." The inclusion of a truly amorphous component into this picture still attracts controversy. Warner et al.[7] proposed a series crystalline/amorphous model, while other authors suggest a single laterally bonded structure with many defects.[4,8]

The microstructure of acrylic fibers arguably has been less extensively studied. The scarcity of investigation of dry-spun fiber in the open literature possibly reflects the lack of microstructure developed in the formation process. In contrast, the rich morphology that can be developed in the spin bath of a wet spinning process has attracted more attention. A good early description of formation/structure relationships primarily for the PAN/dimethylacetamide system was given in 1962 by Craig et al.[9] The freshly coagulated structure was shown to consist of a cellular structure, with nodes of polymer connected by thin rods, the spaces in between forming a porous network. Few workers have attempted to characterize this porous structure and, particularly, the effect of process variables on it.[10,11]

* To whom correspondence should be addressed.

Journal of Applied Polymer Science, Vol. 62, 33–47 (1996)
 CCC 0021-8995/96/010033-15

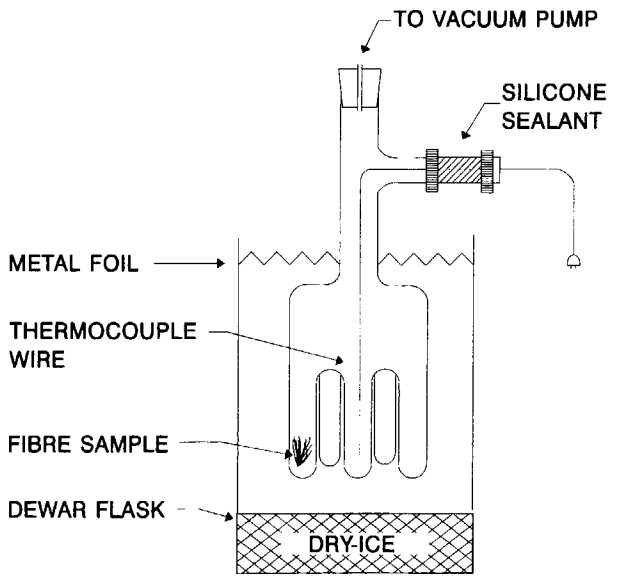

Figure 1 Schematic diagram of the freeze-drying apparatus.

The current work concentrates on the formation and structure of wet-spun acrylic fiber from the sodium thiocyanate solvent system, around which some leading manufacturers operate their acrylic fibers business. The study of as-formed structure and its transformation through the various process steps during manufacture is important for a number of reasons. Courtelle† was one of the first acrylics on the market that is dyed on-line in the gel state. The structure of the substrate plays a key role in the dyeing characteristics of the fiber during this key step.[12] Mechanical properties of produced fiber can determine the ease with which fiber is processed into yarn and then into fabric. These mechanical properties are determined largely by the initial structure that is laid down in the precipitation bath. Characterizing these morphologies has been proven to be a difficult task. In particular, the geometry of fibers makes sample preparation and manipulation for microscopy difficult.

This study introduces a fresh approach to the investigation of wet-spun acrylic structure, which is based on phase-inversion (PI) membrane technology. In flat sheet membrane form, the complications mentioned above can be largely eliminated. Indeed, many aspects of the technology and science underpinning the production of PI membranes is related to the wet spinning of fibers. Additionally, unlike the development of fundamental knowledge of formation/structure/property relationships in wet-spun fibers generally, over recent years, the formation and structure of PI membranes have been developed around a modern polymer theory framework.

† Registered trademark of Courtaulds plc acrylic fiber.

PHASE-INVERSION MEMBRANES

Membrane filtration is rather new as a method of separation. The processes were not considered technically important until about 25 years ago. Today, membrane processes are used in a wide range of applications. This range is matched by the number of different types of membrane, based on material type, and perhaps, more importantly, their morphology.

There exist a number of different membrane preparation techniques. A particular technique is chosen to process and modify a given material, to give the necessary structure which will yield the desired fil-

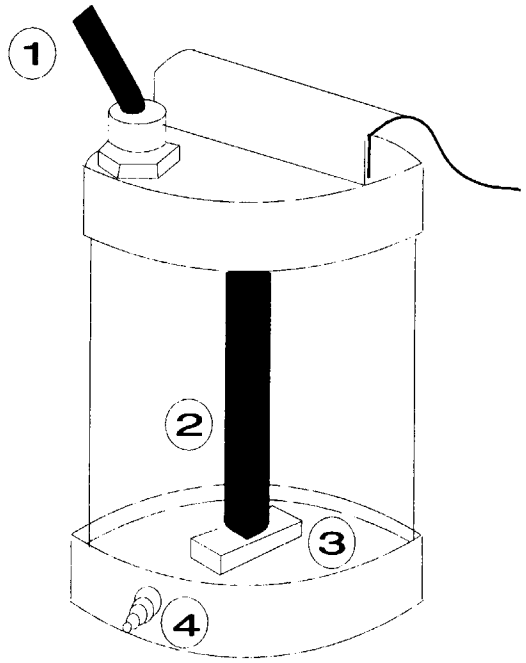

Figure 2 Schematic diagram of the stirred cell for permeability measurements.

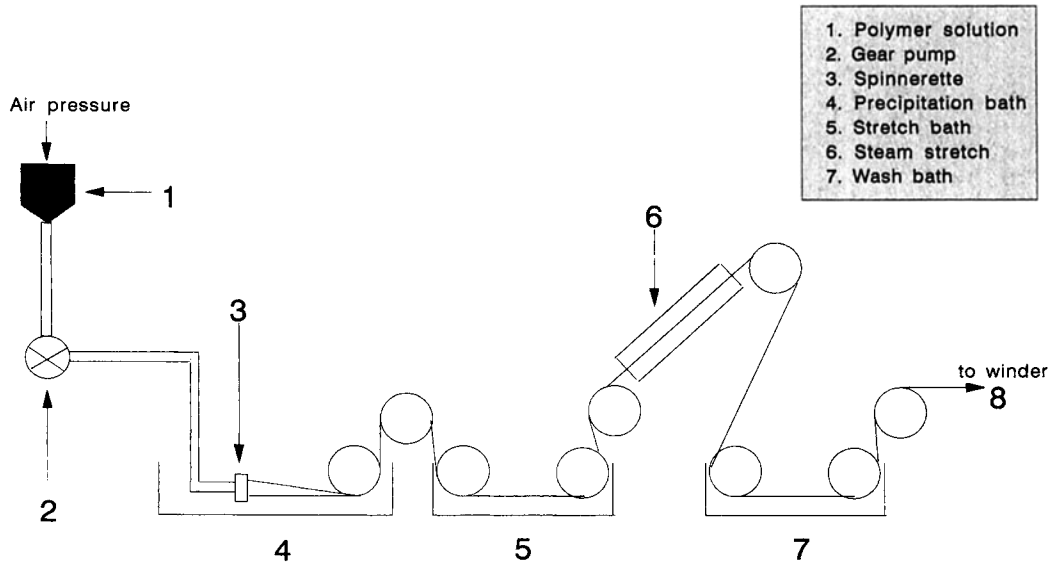

Figure 3 Schematic diagram of the laboratory wet spinning apparatus.

tration performance. This can range from porous membranes (0.1–10 μm) for microfiltration, through graded porous structures (0.001–0.5 μm) for ultrafiltration, to dense skinned types for gas separation and pervaporation. The main preparation techniques include sintering, film stretching, track etching, coating, and phase inversion. Most commercial membranes are obtained by the latter technique.

Flat sheet PI membranes in their simplest form are prepared by casting a polymer dissolved in a solvent upon an inert support and then immersing into a nonsolvent bath. The solvent in the dope and nonsolvent in the bath exchange by diffusion, with the solvent leaving the polymer solution film for the bath, while the nonsolvent enters the film from the bath. After a while, the exchange has proceeded far enough such that the polymer solution becomes thermodynamically unstable, and demixing (phase separation) occurs. Finally, a solid polymer film is formed, containing pores filled with liquid of the composition of the precipitation bath. The structure of the polymer membrane depends on such parameters as the type of solvent and nonsolvent, composition of the casting solution and the precipitation bath, and the temperature of both the casting solution and precipitation bath. In the production of ultrafiltration and reverse osmosis (RO) membranes, formation conditions are employed such that a thin skin of more compact structure on the outside of the membrane is formed. It is this structure which performs the separation duty, giving both acceptable flux rates because of its thinness and selectivity in the small molecule range because of its density. The existence of an outer skin on wet spun acrylic fibers is not widely published, but this work graphically demonstrates one does exist. Indeed, this skin layer can take on as much importance in the processing of wet spun acrylics as it does in membrane technology. The analogy with the wet spinning of fibers is therefore obvious. Even the dimensions (in mass transport terms) tend to be similar for both membranes and wet spun textile fibers, typically 100–300 μm. The obvious dissimilarity arises from the fact that textile fibers are spun at a significant rate through spinneret nozzles, a condition which subjects the polymer solution to both shear and extension forces immediately prior to precipitation. Such a phenomenon is generally not present in flat sheet

Table I Fiber Spinning Conditions

Spin Solution Temp (°C)	Spin Solution Solids (%)	NaSCN in Spin Solution (%)	NaSCN in Precipitant (%)	Precipitation Temperature (°C)	Velocity in Spinneret (*M*/min)	Take-up Velocity (*M*/min)
22	13	45	13.5	−2, 9, 21, 39, 59	12.5	4.0

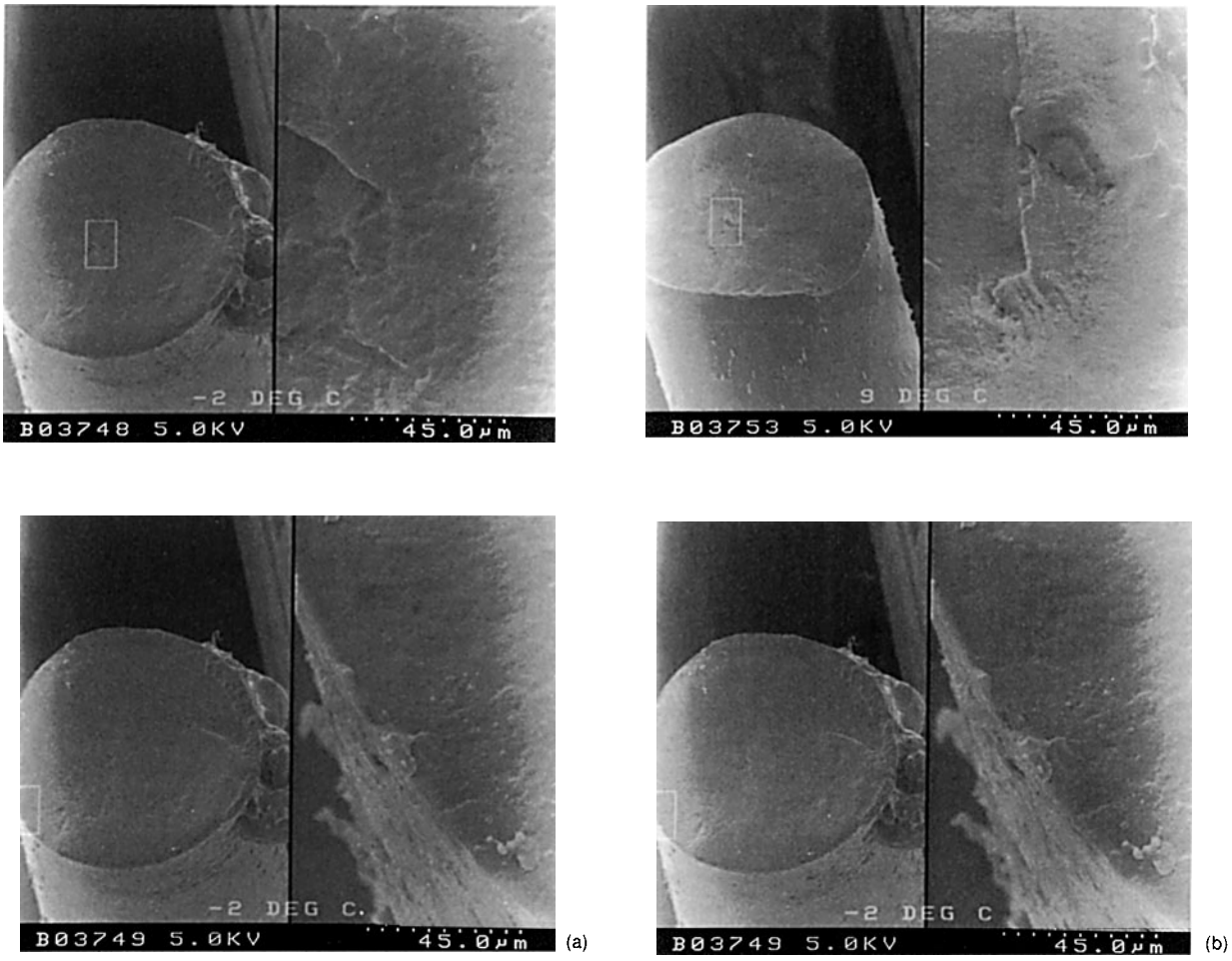

Figure 4 Scanning electron micrograph cross sections of freeze-dried acrylic fibers. Spin bath temperatures (in °C): (a) 59, (b) 39, (c) 21, (d) 9, (e) −2.

PI membrane production. It has therefore been necessary to ascertain whether such in-spinneret processes modify the as-formed structure of wet spun fibers, potentially rendering a direct comparison between the two forms impossible.

EXPERIMENTAL TECHNIQUES

Structure Preservation–Freeze Drying

The porous structure formed in a wet spinning precipitation bath is not at equilibrium and will collapse slowly over time. If the liquid filling the pores is allowed to evaporate, the surface tension forces associated with the creation of fresh liquid–air interfaces expedite the collapse, and much of the original porosity is lost. If drying occurs at elevated temperature, collapse is more complete as polymer mobility is enhanced. Certain characterization techniques require the fiber to be free of liquid, so more elaborate methods to dry the sample are employed.

Freeze-drying has been found to be an effective way of preparing samples with their pore structure intact. A schematic diagram of the apparatus used in this study is shown in Figure 1. In order for the imbibed water to be frozen without significant ice crystal growth, washed samples were first plunged into liquid nitrogen, wherein sample fracture preferably takes place. (Fracturing at room temperature usually leads to significant plastic flow, effectively destroying the underlying structure.) Samples are then transferred to a precooled vessel where evaporation takes place. Suitable sublimation rates were found between −20 and −30°C at a pressure of 10^{-2}–10^{-3} mbar. More importantly, structure preservation is ensured. Total removal of water can be checked by slowly allowing the vessel to warm while monitoring the pressure. If a gradual, but signifi-

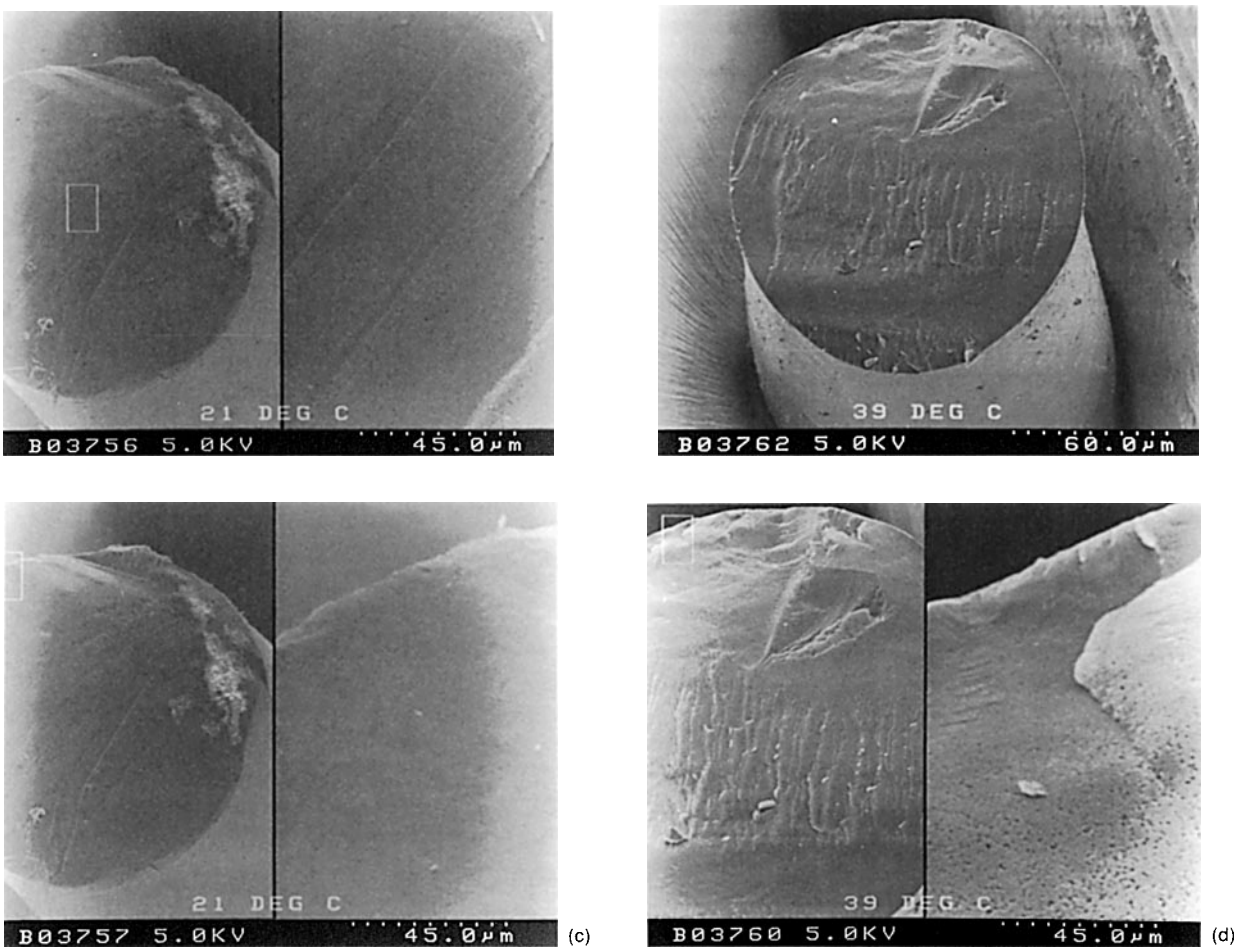

Figure 4 (*Continued from the previous page*)

cant, loss of vacuum is noted, then further drying is required.

Field Emission Scanning Electron Microscopy (FESEM)

Rather than using a tungsten filament to generate electrons, the field emission electron microscope uses a single crystal. This gives a number of advantages over a conventional unit. First, a higher density beam, which gives a better signal to noise ratio at low operating voltage, is produced. This, in turn, allows a lower operating voltage for a given magnification, thus reducing damage of the specimen in the beam. Second, the beam is highly monochromatic, which gives superior resolution. Finally, less coating is required to prevent nonconductive samples from charging. This means that topography is altered to a less degree.

In this work, a Hitachi S4000 FESEM was employed. All samples were gold/palladium-coated to a depth of about 100 Å prior to insertion in the microscope.

Water Imbibition (WI)

While direct observation of the gross structure by FESEM requires a dry substrate, an idea of the total porosity of a sample can be obtained by the simple technique of water imbibition, which can be applied to wet and dry samples alike. The mass of water contained in the water accessible pores is measured and related to the dry fiber mass. A sample of about 0.5 g (dry) weight is immersed in distilled water for 1 h, then placed on a mesh platform of a centrifuge tube. This is then placed in a centrifuge. The top of the tube is covered with Parafilm to minimize water evaporation. The samples are then spun for 6 min at 2400 rpm, equivalent to 550 g. Under these conditions, interstitial water between and around fibers is removed, while water imbibed in the porous net-

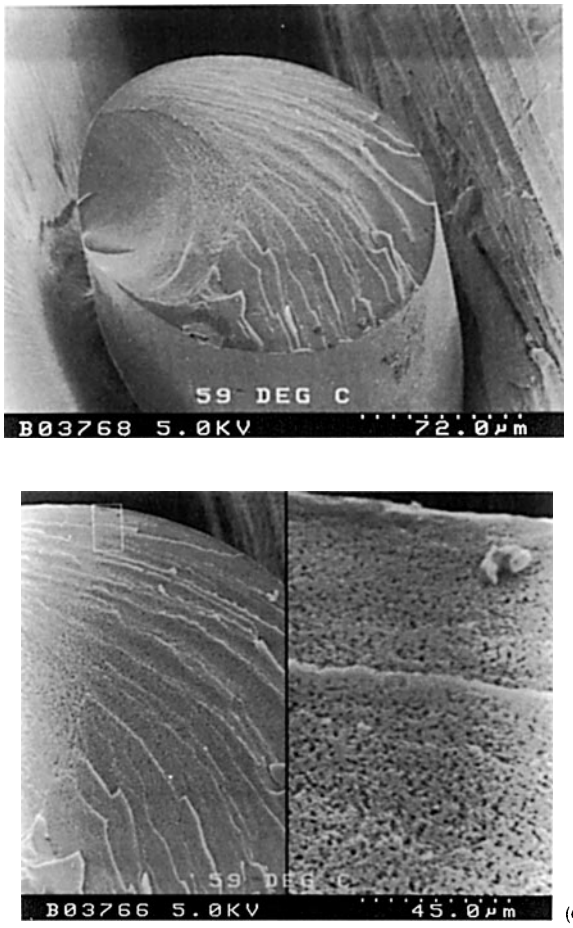

Figure 4 (*Continued from the previous page*)

work remains. After centrifugation, the samples are immediately weighed and dried to constant weight. Water imbibition is then given by the following.

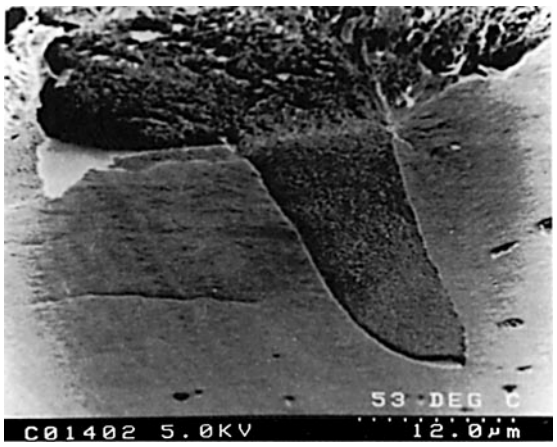

Figure 5 Scanning electron micrograph cross section of freeze-dried acrylic showing skin detachment.

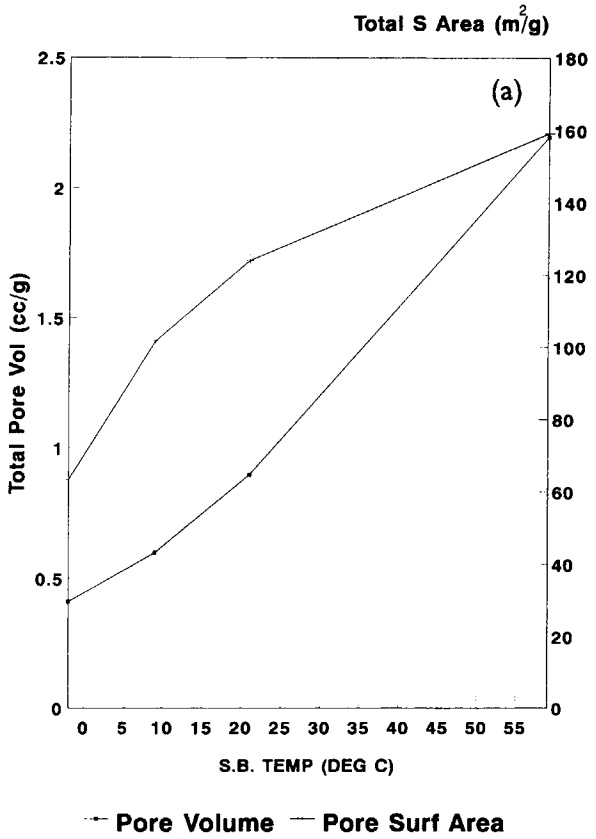

Figure 6 (a) Total pore volume and surface area by mercury porosimetry of freeze-dried acrylic fibers spun at various spin bath temperatures. (b) Cumulative surface area by mercury porosimetry of freeze-dried acrylic fibers spun at various spin bath temperatures.

$$\% \text{ Imbibition} = \frac{\text{weight fiber ex centrifuge} - \text{dry fiber weight}}{\text{dry fiber weight}} \times 100$$

Hydraulic Permeability

Hydraulic permeability is used extensively in the membrane industry to characterize the flux of permeants through ultrafiltration, reverse osmosis, and microfiltration membranes. In a typical experiment, pure water is pumped through a hollow fiber or flat sheet of known dimensions at a given pressure, and the volumetric rate of permeating water is measured. This gives a relative measure of the likely flux rate in use. In terms of membrane structure, the measurement gives an idea of the combination of level of porosity and average pore size in the skin layer, which represents the greatest barrier to flow. This technique then discriminates between the important skin layer and the bulk of the structure. On a more

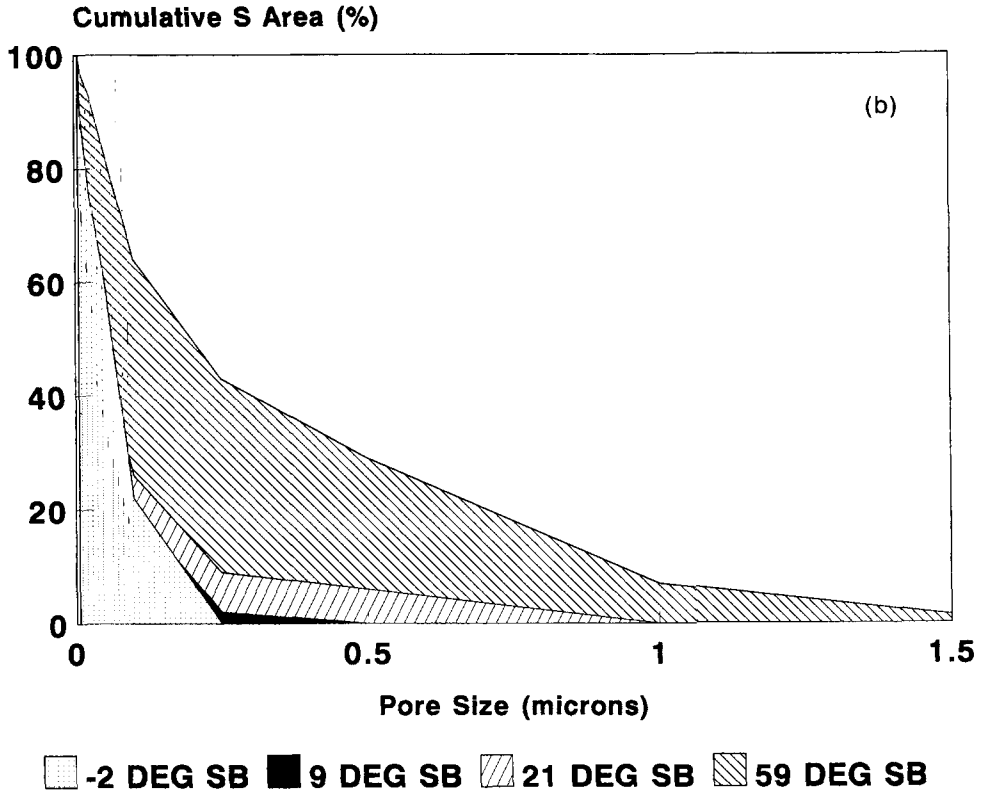

Figure 6 *(Continued from the previous page)*

fundamental level, by varying the pressure and measuring flow rate, a pore size distribution can be calculated, provided some assumptions are made about the geometry of pores. The Hagen–Poiseulli equation, for instance, assumes that pores are cylindrical.

$$J = \frac{\varepsilon r^2}{8\eta\tau}\frac{\Delta P}{\Delta x}$$

where J is the flux at a pressure ΔP through a membrane of thickness Δx; r is the average pore radius, η, the liquid viscosity; ε, the membrane porosity; and τ, the tortuosity factor.

At low pressure, only the largest pores are accessible and, as the pressure is increased, smaller and smaller pores contribute to the flux until all pores are permeable. Now, the flux rate increases linearly with pressure according to the Hagen–Poiseuille equation.

Never-dried film samples were placed on the sintered glass support of a 10 mL stirred cell (Model S2278 from Sigma–Aldrich; see Fig. 2), and the cell closed. Deionised and filtered (Millipore) water was quickly transferred to the cell, and the cell filled. A pressure of one bar from a regulated air supply was applied to the top of the cell, the magnetic stirrer started, and the permeate collected over time. Hydraulic permeability (L_p) is given by the following equation:

$$L_p = \frac{V}{Atp}$$

where V is the volume of permeant collected; A, the membrane area; t, the time interval; and p, the applied pressure.

Mercury Porosimetry

The use of this technique to study structure in textile fibers has been extensively reviewed by Quynn.[13] Essentially, in this technique, mercury is incrementally forced under pressure into the porous structure of a dry sample. At each incremental pressure, the volume of mercury introduced into the sample is accurately measured. From the Laplace equation,

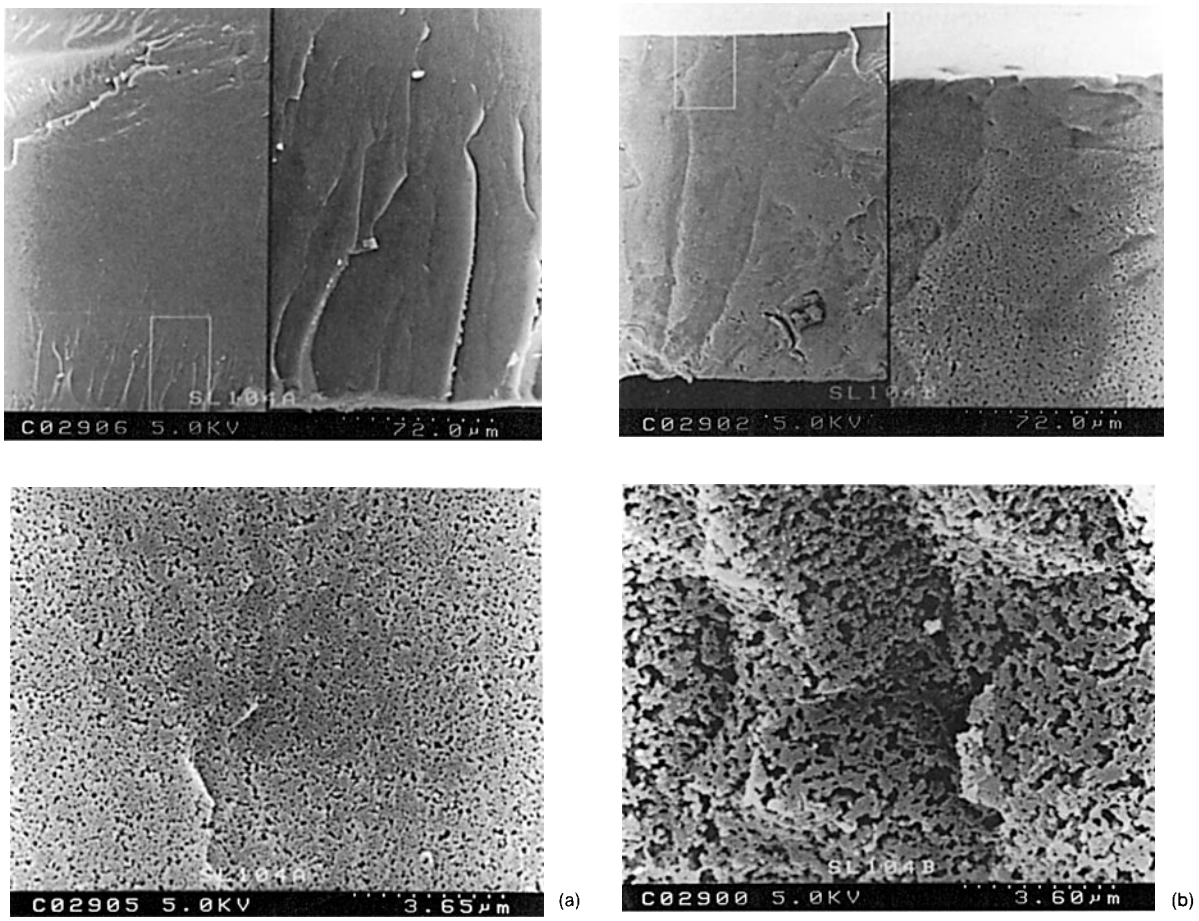

Figure 7 (a) Scanning electron micrograph cross section of freeze-dried cast acrylic film precipitated at 21°C in 13.5% aqueous NaSCN. (b) Scanning electron micrograph cross section of freeze-dried cast acrylic film precipitated at 48°C in 13.5% aqueous NaSCN.

$$r_p = \frac{2\gamma}{\Delta P} \cos \theta$$

where r_p is the pore radius; γ, the surface tension of the liquid; θ, the contact angle; and ΔP, the applied pressure. For each pressure, a pore volume relating to a particular pore diameter can be calculated, leading to a pore size distribution. This calculation assumes that the pores are simple capillaries. In this work, a Micromeritrics Model 9310 was used to probe the open pore structure of freeze-dried fiber samples. Samples of 0.02–0.1 g were used in a 3 cm^3 powder penetrometer. This ensured that fibers were not lost in evacuation prior to mercury intrusion.

Pore diameters in the range several microns to 0.006 μm are accessible to the Micromeritics Model 9310. The output is total pore volume, total surface area, and incremental pore volume and surface area as a function of pore diameter.

Polarized Infrared Microspectroscopy

The use of polarized infrared spectroscopy to measure the degree of chain orientation in polymers has been described elsewhere.[14] By measuring the absorbance of characteristic groups in directions which are parallel and perpendicular, respectively, to some defined process direction, the level of orientation of chains can be calculated.

In this work, experiments were performed with a Nicolet 740 Fourier Transform Infrared (FT-IR) spectrometer, with a Spectra Tech wide-grid polarizer. Samples were observed with the electric vector parallel to the machine direction (made obvious from surface striations), and perpendicular to it. Background spectra were also recorded under identical conditions. The orientation of PAN chains was determined from the dichroic ratio of the nitrile stretching vibration at 2244 cm^{-1} as followed in another work.[15]

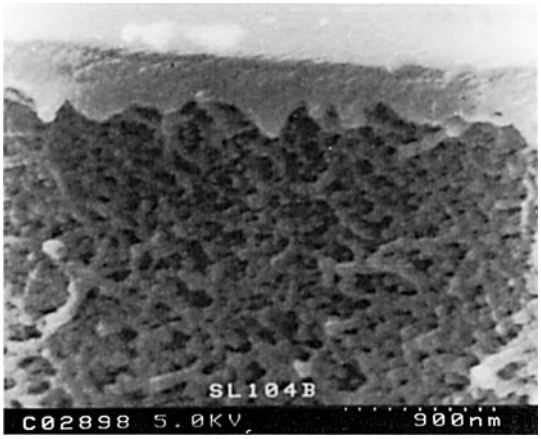

Figure 8 Scanning electron micrograph cross section of freeze-dried cast acrylic film precipitated at 48°C, showing skin.

FIBER SPINNING AND MEMBRANE CASTING

Fibers were produced on a laboratory spinning line, a schematic diagram of which is shown in Figure 3. The acrylic polymer used throughout this work was a poly(acrylonitrile) copolymer containing a 6% (by weight) neutral comonomer and a 1% (by weight) sulphonic acid dyesite comonomer. Polymer solution contained in pot (1) is fed via a gear pump (2) through lagged pipework to the spinneret head (3). The spinneret contains 200 holes, with each one 75 μm in diameter. The nascent filaments travel through a precipitation bath (4), the contents of which are circulated in a loop, onto a take-up godet. From here, stretching is possible through bath (5), which can circulate hot water, with further stretching possible through a tunnel (6), into which low pressure steam is injected. The filaments are washed free of solvent in bath (7), and wet fiber is finally collected on a spool (8). Conditions used are shown in Table I.

Extruded membranes were produced on the same spinning line, but the spinneret was replaced with a slot jet, with slit dimensions of 5 cm $\times$ 100 μm. A single precipitant temperature of 50°C was employed. The polymer solution throughput used gave a shear rate in the die of 79,000 sec^{-1}, somewhat higher than that for the fiber case (24,000 sec^{-1}). This difference would not be expected to give rise to different structures in the flowing polymer solution, as the fluid exhibits a smooth power law relating shear viscosity to shear rate. The take-up speed was adjusted to give a jet stretch ratio (extrusion velocity divided by take-up velocity) of about 0.4, similar to 0.32 for the fiber case.

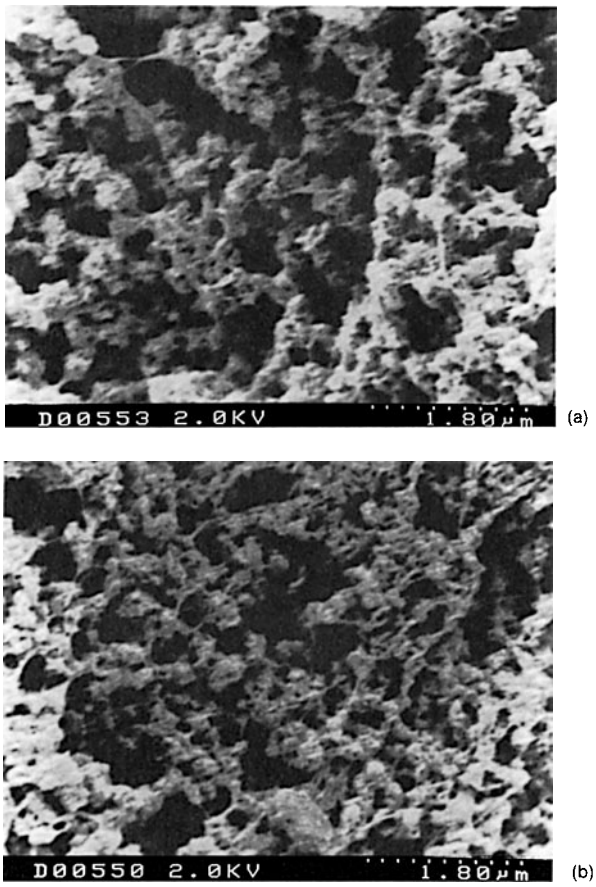

Figure 9 (a) Scanning electron micrograph cross section perpendicular to the extrusion direction of freeze-dried extruded acrylic film. (b) Scanning electron micrograph cross section parallel to extrusion direction of freeze-dried extruded acrylic film.

Cast membranes were produced in the conventional manner by dragging a smooth bar with wire of known gauge wound around it slowly over a poly-

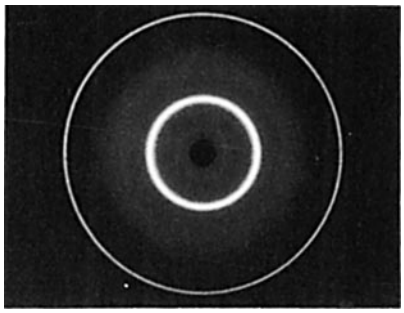

Figure 10 WAXRD flat plate photograph of freeze-dried unstretched fiber, precipitated at 59°C.

mer solution pool sitting on a glass plate. The glass plate was then immersed face down onto supports inside a vessel containing precipitant. In this way, the heavier solvent which diffuses from the film falls away from the coagulating polymer. Coagulation temperatures of 3, 12, 21, 35, and 48°C were used for membrane formation.

For experiments away from ambient temperature, a jacketed dish was used.

RESULTS AND DISCUSSION

Microscopy and Porosimetry

Figure 4(a–c) shows a series of cross sectional SEMs of undrawn acrylic fiber spun at increasing coagulation temperature. Note that the scale bar refers to the least magnified image, while the inset is ten times this magnification. Here, the two-phase structure typical of nonsolvent induced precipitation can be noted, particularly for the structures precipitated at the higher temperatures. An isotropic network of polymer comprises the filaments, interspersed with a pore network, which, at the point of formation, would have been filled with precipitant. There appears to be an increase in porosity of as-formed structure with increasing coagulation temperature, based on pore size and filament diameter. This is in agreement with previous work on acrylic fibers.[10] The effect is quantified by porosimetry discussed below. The gradual increase in pore dimensions from the periphery to the interior of the fibers can also be noted, particularly in those samples formed at higher temperature. A final point worth noting is the very dense skin on the outside of the filament. Figure 5 shows this graphically, where the skin layer has torn away from the underlying structure.

The characterization of these pore structures by mercury porosimetry is indicated in Figure 6. The first part of this figure shows quantitatively how pore volume and surface area increases with increasing temperature, confirming observations from micrographs. Figure 6(b) gives an indication of pore size distribution, showing that those structures precipitated at higher temperature have a pore size distribution centered at larger pore diameter.

Figure 7(a,b) shows micrographs of cast films coagulated at 21 and 48°C. The magnifications are not exactly matched, but the similarity in structure to the related extruded fibers is evident. Figure 8 shows that a dense outer skin is also present on the surface of the film, which was in contact with the precipitant.

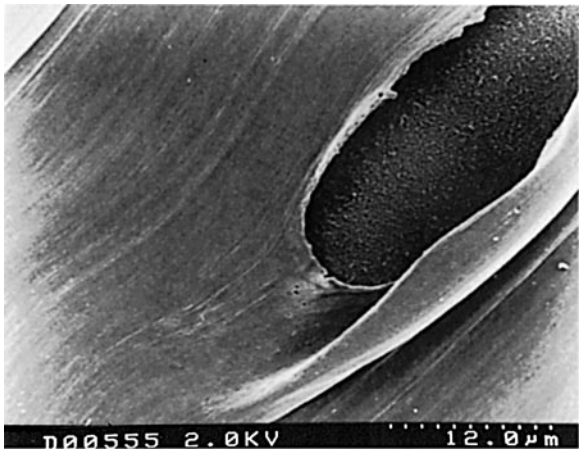

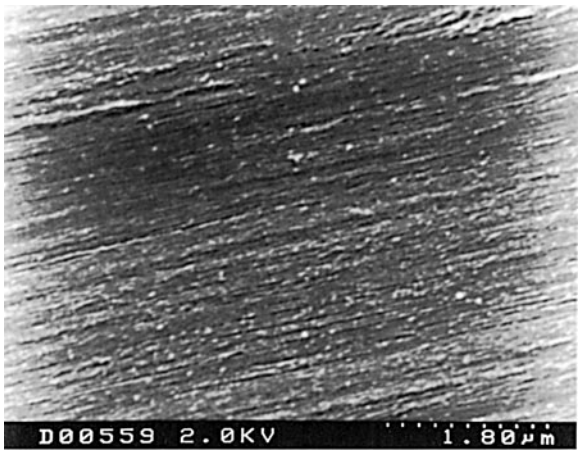

Figure 11 Scanning electron micrograph of the surface of freeze-dried extruded acrylic film.

The formation of such a graded structure has been rationalized by several authors working in the membrane field. Probably, the most satisfying description has been furnished by Reuvers et al.[16] They argue that skin formation is a result of a very fast outflow of solvent from the outside of the polymer film into the bath, compared to a slower inflow of nonsolvent into the film. This occurs because solvent leaving the film can diffuse quickly into the bath, which maintains the concentration gradient at the interface, while nonsolvent entering the film cannot diffuse as quickly into the bulk of the film. Consequently, the concentration gradient of water at the interface is very quickly reduced. Since solvent leaves the polymer solution in relatively greater quantity, the concentration of polymer at the interface increases. Hence, when instability is reached, phase separation proceeds from a higher polymer concentration than the bulk, and a denser structure

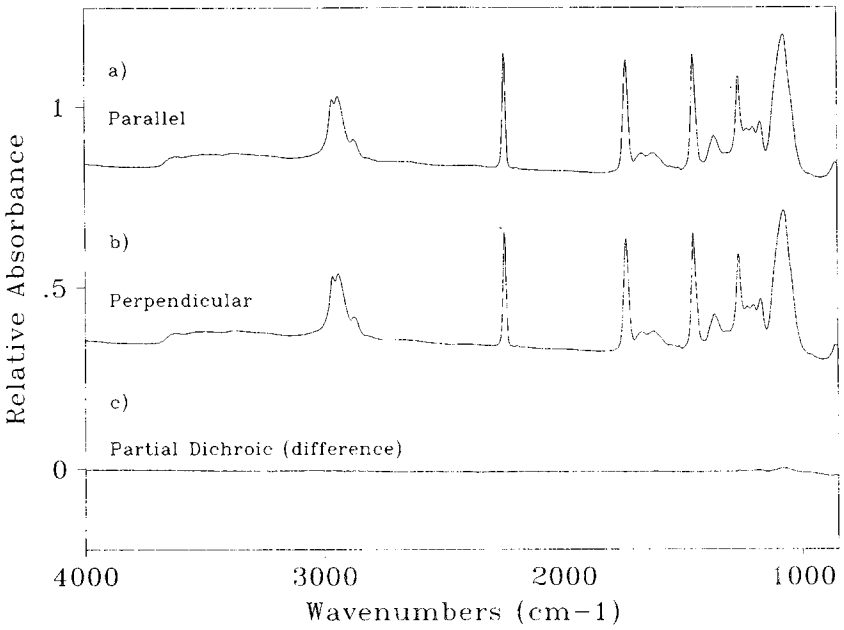

Figure 12 FT-IR spectra of freeze-dried skin taken from extruded acrylic film: (a) electric vector parallel to extrusion direction, (b) electric vector perpendicular to extrusion direction, and (c) partial dichroic spectrum (difference spectrum).

is formed.[17] After formation of this skin layer, further diffusion across the interface is mediated by the skin, and the graded structure beneath is formed as a consequence of the relative rates of diffusion across the skin and the effect that this has on local polymer concentration at the point of instability.

A study of the kinetics of phase separation for this system has been attempted, following the

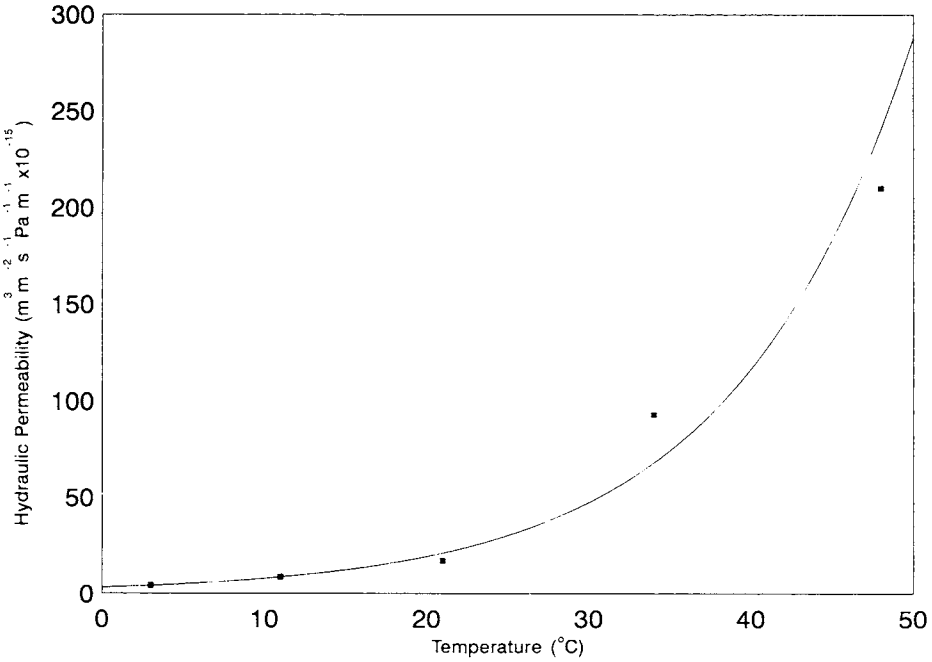

Figure 13 Hydraulic permeability of acrylic films (normalized to thickness) precipitated in 13.5% aqueous NaSCN at a range of temperatures.

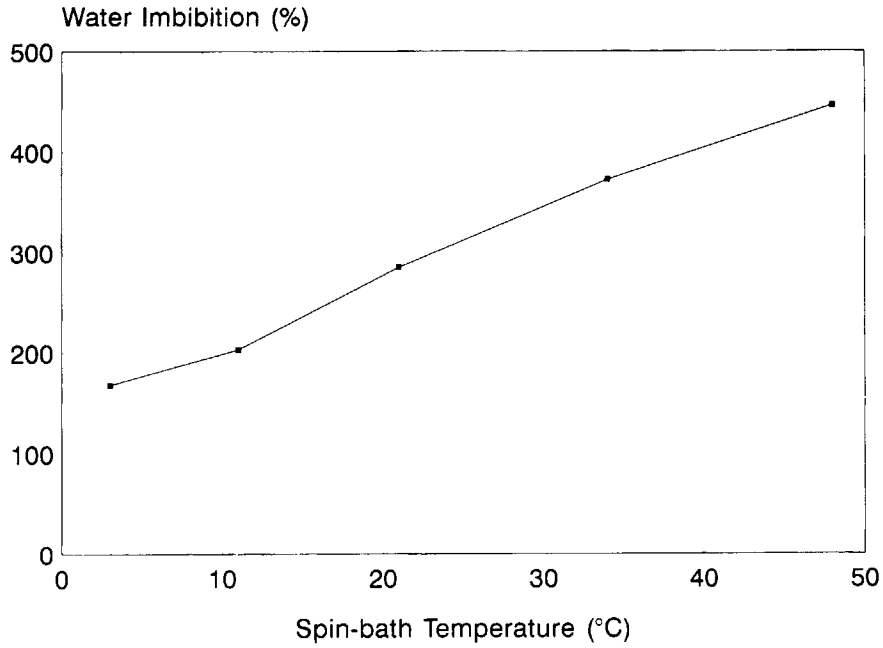

Figure 14 Water imbibition values of acrylic films precipitated in 13.5% aqueous NaSCN at a range of temperatures.

methodology of Reuvers et al.[16] Details will be published in a separate paper.

Cross sections of extruded film in both the transverse and parallel (to the extrusion direction) are shown in Figure 9(a) and 9(b), respectively. As found by Craig et al.,[10] the extrusion operation appears to impose no orientation on the microstructure. Figure 10, showing a WAXRD flat plate photograph of an as-formed (extruded) fiber, supports this view.

However, the micrograph of the surface of an extruded film (showing damage by manipulation) in Figure 11 suggests that some part of the outer surface may have a level of orientation resulting from the extrusion. It is known for polymer chains in solution under the action of high shear forces to orientate in the direction of the flow.[18] The precipitation of polymer, particularly at the outside of a filament or film, is known to be extremely rapid in such systems; and despite the fact that relaxation of stresses developed in the die occurs on exit into the bath, it is possible that at the very outer surface, some level of flow induced orientation is frozen in by rapid precipitation. To characterize the level of orientation of this very thin layer *in situ* is probably beyond the resolution of conventional techniques, even infrared attenuated total reflectance (ATR) techniques, which has been used to depth profile polymer films.[19] However, it was found possible to remove the dense skin while the sample was still wet with fine tweezers to produce samples large enough for polarized infrared microspectroscopy. Wet samples were attached to barium fluoride spectrometer windows with adhesive tape, leaving a small area uncovered for penetration by the infrared radiation. The sample was then freeze-dried before observation in the FT-IR spectrometer. Figure 12(a,b) show spectra from scans with the electric vector parallel and perpendicular, respectively. A difference spectrum is shown in Figure 12(c). Clearly, the partial dichroic spectra are identical, indicating complete isotropy. The apparent skin layer orientation suggested by the striations on SEM micrographs may be the result of a poorly finished internal surface of the capillary section of the slit die. This level of structure is generally not present on fibers spun under similar conditions.

The lack of orientation is perhaps surprising in the light of previous work. Paul[20] noted an increase in sonic modulus with increasing jet stretch ratio for fibers spun from the DMAC system. At the jet stretch ratio of around 0.5 used in this work, Paul found an orientation factor in the region of 0.3.

Hydraulic Permeability

The effect of precipitant temperature on the permeability of cast acrylic membranes can be seen in Figure 13. These permeabilities are normalized to film thickness, as the increased porosity with pre-

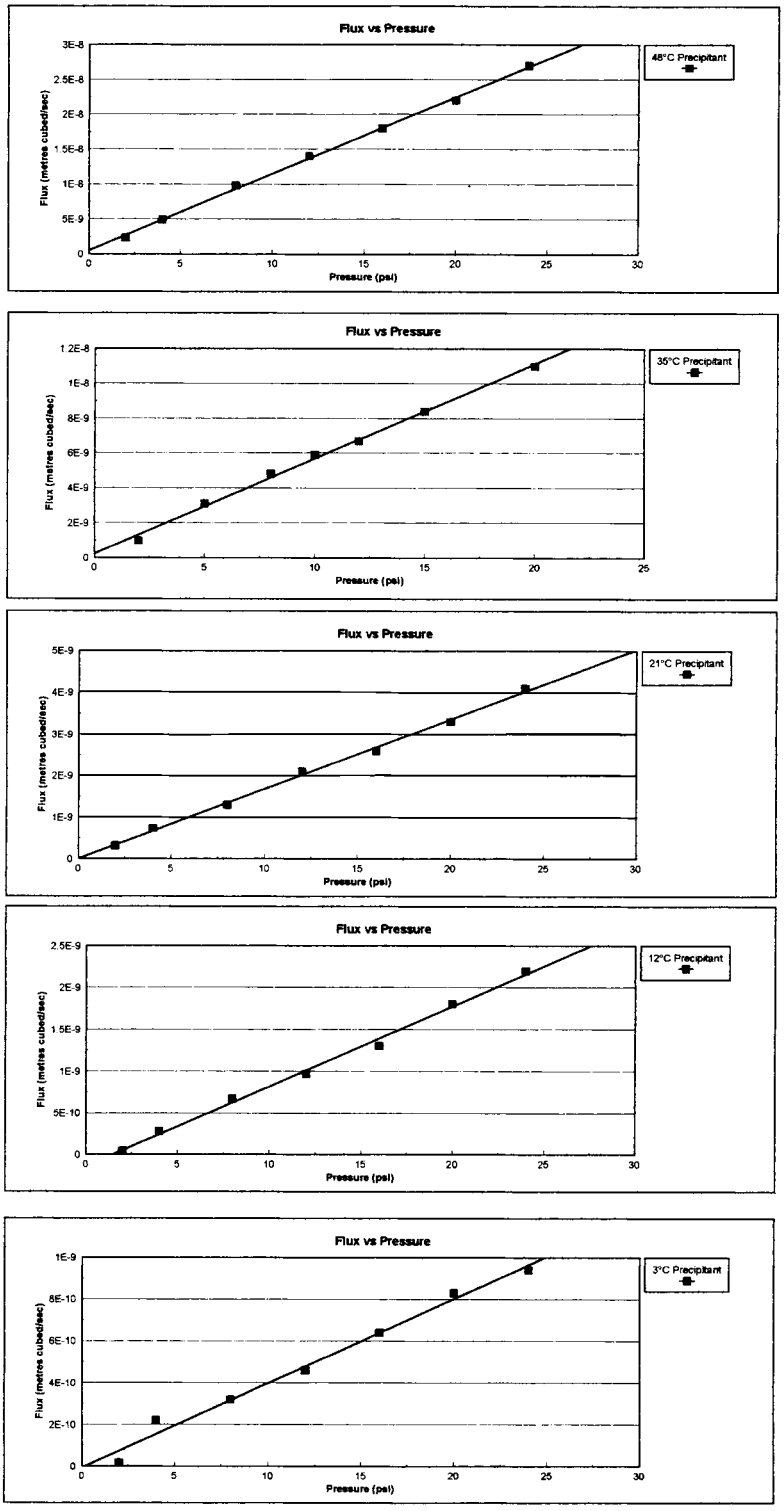

Figure 15 Water flux rate as a function of transmembrane pressure of acrylic films precipitated in 13.5% aqueous NaSCN at a range of temperatures.

Table II Average Pore Radius Calculated from Permeability Data

Precipitant Temp (°C)	Average Pore Radius (n*M*)
3	6.5
12	9.6
21	13.9
35	42.8
48	64.2

cipitation temperature serves to thicken the film. In the absence of any gross change in pore type, these results are indicative of an increase in porosity and/or an increase in average size of pores and will relate most strongly to the denser top layer.

Water imbibition values for the same samples are shown graphically in Figure 14, and, like mercury intrusion data for fibers, indicate an increase in total porosity with increasing precipitant temperature. It appears, therefore, that both bulk and skin porosity is increasing with precipitant temperature.

Figure 15 shows flux rate as a function of transmembrane pressure for each membrane. The linear relationships allow the application of the Poisseuille equation to generate average pore radii. Using water imbibition values as a measure of total porosity, and membrane thicknesses measured using a sensitive Ames Gauge, pore radii calculated from the permeability results are presented in Table II. The value for the film precipitated at 48°C falls in the range indicated in a SEM of the upper surface of the same film (Fig. 16). While it is difficult to extract accurate pore sizes from such micrographs, an approximate evaluation is possible.

A hydraulic permeability value of 1.3×10^{-13} m^3 m^{-2} Pa^{-1} s^{-1} m^{-1} was measured for the extruded film precipitated at 50°C. This is lower than for the equivalent cast film value of 2.1×10^{-13} m^3 m^{-2} Pa^{-1} s^{-1} m^{-1}, extracted from Figure 13. It should be borne in mind though that the extruded film has a double skin in that the two faces of the film are exposed directly to precipitant. In the case of the cast film, only the upper surface is exposed directly to precipitant, and only one skin layer forms. Because of this, the permeability data of extruded and cast films cannot be compared. However, since it has been shown that the skin layer could be removed for characterization, hydraulic permeability values were obtained for an extruded film with first one surface removed, then with both surfaces removed. Table III summarizes the L_p values and indicates the important influence the skin layer has on the permeability of water. Note that these results are again normalized to film thickness. For the skin-removed films, the original film thickness has been used since no measurable thickness change could be measured on their removal. The micrograph of a fiber with partially detached skin in Figure 5 supports this, illustrating just how thin the top layer is. The value for an extruded film with one top layer removed falls in the area for cast films precipitated at the same temperature, which suggests that the effect of extrusion has a negligible effect, in particular, on the surface porosity.

This is in contrast to recent work reported by Shilton et al. for polysulphone hollow fibers.[21] The permeability and selectivity of CO_2/CH_4 mixtures was found to increase with increasing shear rate. Shilton et al. rationalize this behavior in terms of a greater alignment of chains at the spinneret wall, which is locked in as the nascent fiber coagulates.

In terms of Courtelle acrylic fibers, the permeability of the skin layer is an important effect. A significant proportion of fiber produced is dyed online; and in a short space of time, the dye species have to penetrate first the skin layer before dyeing the bulk of the filament. To illustrate this, in a laboratory experiment, a hank of fiber with no free ends dyed to give 2.6% dye on dry weight of fiber in 60 sec at 20°C. In contrast, chopped fiber of similar mass dyed to give 4% dye on fiber in the same time. In the former case, dye molecules or associates have to travel through the skin layer in order to permeate the internal porosity and reach dye sites; while in the latter, there is immediate access to internal porosity through fiber ends.

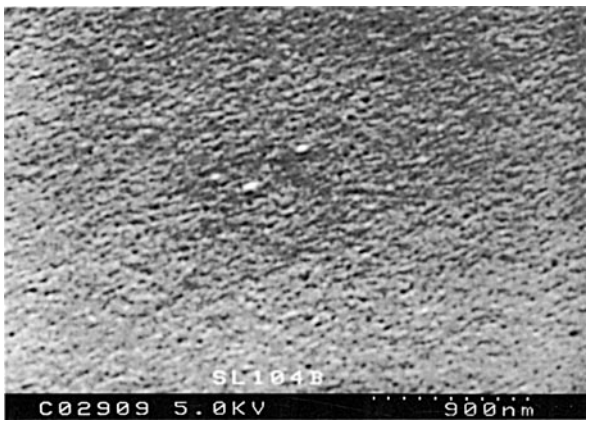

Figure 16 Scanning electron micrograph of the surface of cast acrylic film precipitated at 48°C in 13.5% aqueous NaSCN.

Table III Hydraulic Permeability Values

Sample	L_P ($\times 10^{-13}$ m^3 m^{-2} Pa^{-1} s^{-1} m^{-1}) (normalized to 1 m thickness)
Extruded film coagulated at 50°C	1.3
As above with one skin layer removed	1.8
As above with both skin layers removed	3.5

CONCLUSIONS

The value of using membrane geometry and techniques to study the microstructure of wet-spun acrylic fibers from the aqueous sodium thiocyanate system has been demonstrated. This approach will be applicable to other wet spinning systems provided there is no interaction between the extrusion process and formed fiber morphology. In such cases, where there is, extruded membranes could usefully serve as fiber analogues.

One membrane characterization technique not reported here, which could prove useful in the characterization of wet-spun fibers, is the molecular weight cut off. This parameter is defined as that molecular weight of a permeating solute, which is 90% rejected by the membrane. In reality, it is not an absolute measure of selectivity as the behavior will clearly be dependent on the size and shape a particular solute adopts in the solution and on any interaction effects between the solute and substrate. Further, systematic research would need to be carried out to define a suitable technique for acrylic membranes.

By comparing the morphology of cross sections in transverse and parallel directions of extruded film, it has been confirmed that the microstructure formed in the precipitation bath is isotropic. Hydraulic permeability measurements have been used to calculate an average pore dimension in the skin layer. The calculated values for membranes precipitated at different temperatures lie in the range suggested in electron micrographs of the surface.

The existence of a dense skin on the outer surface of fibers is a result of immersion into a nonsolvent. In this system, the skin layer has been shown to be isotropic by a novel polarized infrared microspectroscopy technique. The extruded skin offers the same resistance to water flow as a skin formed under quiescent flow conditions. Furthermore, the skin has been shown experimentally to exert a strong influence on the permeation of water (and dye molecules), in keeping with accepted membrane knowledge. This is of profound importance in the gel dyeing of wet-spun acrylic fibers.

The authors thank Steve Church and Tony Hyde, both of Courtaulds Corporate Technology, for the infrared and scanning electron microscopy, respectively, and Courtaulds Corporate Technology for supporting this work and granting permission to publish.

REFERENCES

1. J. Grobelny, M. Sokol, and E. Turska, *Polymer*, **25,** 1415 (1984).
2. K. Kamide, H. Yamazaki, K. Okajima, and K. Hikichi, *Polym. J.*, **17**(12), 1233 (1985).
3. G. Svegliado, G. Talamini, and G. Vidotto, *J. Polym. Sci.*, **A15,** 2875 (1967).
4. C. R. Bohn, J. R. Shaefgen, and W. O. Sratton, *J. Polym. Sci.*, **55,** 531 (1961).
5. R. D. Andrews and R. M. Kimmel, *J. Polym. Sci. Polym. Lett.*, **3,** 167 (1965).
6. A. K. Gupta and N. Chand, *Eur. Polym. J.*, **15,** 899 (1979).
7. S. B. Warner, D. Uhlmann, and L. Peebles, *J. Mat. Sci.*, **10,** 758 (1975).
8. P. H. Lindenmeyer and R. Hoseman, *J. Appl. Phys.*, **34,** 42 (1963).
9. J. P. Craig, J. P. Knudsen, and V. F. Holland, *Text. Res. J.*, **32,** 6,435 (1962).
10. J.P. Knudsen, *Text. Res. J.*, **33,** 13 (1963).
11. K. Terada, *Sen'i Gakkhaishi,* **29,** T451 (1973).
12. R. Jenny, Paper Given at 27th Intl. Man-Made Fibre Congress, Dorndim, Austria, Sept. 1988.
13. R. G. Quynn, *Text. Res. J.*, **33,** 21 (1963).
14. B. Jasse and J. L. Koenig, *J. Macromol. Sci. Rev. Macromol. Chem.*, **C17**(1), 61 (1979).
15. Z. Bashir, A. R. Tipping, and S. P. Church, *Polymer Intl.*, **33,** 9 (1994).
16. A. J. Reuvers, J. W. A. van den Berg, and C. A. Smolders, *J. Mem. Sci.*, **34,** 45 (1987).
17. C. A. Smolders, J. J. Van Aartsen, and A. Steenbergen, *Kolloid Z. Z. Polym.*, **243,** 14 (1971).
18. M. R. Mackley, *J. Polym. Sci. Polym. Symp.*, **73,** 75 (1985).
19. J. P. Hobbs, C. S. P. Sung, K. Krishnan, and S. Hill, *Macromols*, **16,** 193 (1983).
20. D. R. Paul, *J. Appl. Polym. Sci.*, **13,** 817 (1969).
21. S. J. Shilton, G. Bell, and J. Ferguson, *Polymer*, **35**(24), 5327 (1994).

Received October 6, 1995
Accepted March 19, 1996